Impurity-doped kagome antiferromagnet: A quantum dimer model approach

Didier Poilblanc[1] and Arnaud Ralko[2]
[1]*Laboratoire de Physique Théorique, UMR5152, CNRS and Université de Toulouse, Toulouse, F-31062, France*
[2]*Institut Néel, UPR2940, CNRS and Université de Grenoble, Grenoble, F-38000, France*
(Received 4 October 2010; published 19 November 2010)

The doping of quantum Heisenberg antiferromagnets on the kagome lattice by nonmagnetic impurities is investigated within the framework of a generalized quantum dimer model (QDM) describing (a) the valence-bond crystal (VBC), (b) the dimer liquid, and (c) the critical region on equal footing. Following the approach by Ralko *et al.* [Phys. Rev. Lett. **101**, 117204 (2008)] for the square and triangular lattices, we introduce the (minimal) extension of the QDM on the kagome lattice to account for spontaneous creation of *mobile* $S=1/2$ spinons at finite magnetic field. Modulations of the dimer density (at zero or finite magnetic field) and of the local field-induced magnetization in the vicinity of impurities are computed using Lanczos exact diagonalization techniques on small clusters (48 and 75 sites). The VBC is clearly revealed from its pinning by impurities, while, in the dimer liquid, crystallization around impurities involves only two neighboring dimers. We also find that a next-nearest-neighbor *ferromagnetic* coupling favors VBC order. Unexpectedly, a small-size spinon-impurity bound state appears in some region of the dimer-liquid phase. In contrast, in the VBC phase the spinon delocalizes within a large region around the impurity, revealing the weakness of the VBC confining potential. Lastly, we observe that an impurity concentration as small as 4% enhances dimerization substantially. These results are confronted to the valence-bond glass scenario [R. R. P. Singh, Phys. Rev. Lett. **104**, 177203 (2010)] and implications to the interpretation of the nuclear magnetic resonance spectra of the Herbertsmithite compound are outlined.

DOI: 10.1103/PhysRevB.82.174424 PACS number(s): 75.10.Jm, 05.30.−d, 05.50.+q

I. INTRODUCTION

The spin-1/2 quantum Heisenberg antiferromagnet (QHAF) on the kagome lattice [see Fig. 1(a)] is believed to be the paradigm of frustrated quantum magnetism. It is also the best candidate to observe exotic (nonmagnetically ordered) phases predicted by theorists. Among those, an algebraic spin liquid,[1] a gapped dimer or spin liquid[2,3] or a number of valence-bond crystals (VBC) with 12-site,[4] 18-site,[5] and 36-site[5–7] unit cells or with columnar dimer order[8] have all been proposed as possible ground state (GS) of the kagome QHAF.

On the experimental side, Herbertsmithite[9] is an almost perfect realization of a kagome QHAF. In this material copper atoms carrying spin-1/2 degrees of freedom (oxidation state +2) are located on the sites of (very weakly coupled) kagome layers. In addition to the crystallographic structure, the closeness to an ideal system is supported by the remarkable *absence* of any magnetic ordering at the lowest attainable temperatures,[10] as expected for a highly frustrated quantum magnet.

However, small deviations from a perfect kagome QHAF are known in this material. In addition to a small Dzyaloshinskii-Moriya (DM) anisotropy,[11] Herbertsmithite contains a small amount of nonmagnetic zinc impurities substituting copper atoms in the kagome planes. Nuclear magnetic resonance (NMR) offers a fantastic tool to probe impurities via the change induced by a nearby impurity on the local magnetic field at the nucleus whose resonance is being measured. The first estimations from NMR (Ref. 12) of the zinc concentration range from 6% to 10%. It is not clear therefore, which experimental features in Herbertsmithite can really be attributed to intrinsic properties of the kagome QHAF and which of them are induced, e.g., by zinc substitution.

One of the strong motivations of this work is to investigate the effect of spinless impurities in quantum disordered

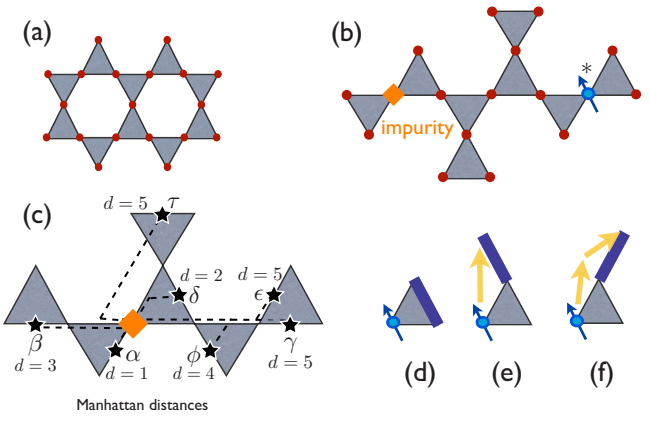

FIG. 1. (Color online) (a) Kagome lattice consisting of a hexagonal lattice of corner-sharing frustrated triangular units. The Heisenberg AFM interaction acts on all bonds of every triangle. (b) A nonmagnetic static impurity (lozenge) in the kagome lattice is described as a vacancy. Mobile spinons (arrows) carry spin-1/2 degrees of freedom. (*) The $N=75$ cluster contains only a single impurity and no spinon. (c) The Manhattan distance d is obtained by counting the number of unit segments (oriented along the two crystallographic axis) on the path joining the impurity to a given bond center. Nonequivalent bonds are labeled by greek letters. (d) A spinon (carrying spin-1/2 shown by a blue arrow) on a triangle cannot hop on the sites of the same triangle. (e) and (f) A spinon can hop at further distances leading to a 120° (c) or 180° (backflow) rotation (d) of the involved dimer.

(i.e., nonmagnetic) phases which are the most serious candidates for the Herbersmithite GS. Starting from a simple description of this material in terms of a SU(2)-symmetric kagome spin-1/2 QHAF (neglecting the small DM anisotropy) recent calculations of NMR spectra[13] seem to reflect key experimental features.[12] On the other hand, the local susceptibilities (Knight shifts) obtained by high temperature series expansion[14] were claimed to agree with an algebraic (gapless) spin-liquid phase. Here we provide an alternative analysis based on a generalized quantum dimer model (QDM) which can naturally describe (a) topological (so-called $\mathbb{Z}_2$) spin-liquid, (b) VBC, and (c) the critical region on equal footing and distinguish features around impurities which are specific to each phase. The paper is organized as follow: first, in Sec. II, we describe the QDM framework, the modeling of the static dopants and the simplest extension of the QDM to account for a small magnetization (induced by a finite magnetic field) in the ground state. In Sec. III, the results for a single imbedded impurity are described. This includes the investigation of the pinning of the VBC and the calculation of the spin density of a doped mobile spinon around the vacancy. Then, in Sec. IV we move on to the case of several impurities and show how the dimerization pattern can be enhanced. A discussion of the experimental NMR data in the light of our results is given in Sec. V as well as some concluding remarks in Sec. VI.

II. THEORETICAL DESCRIPTION

A. Impurities described as vacancies

Let us first discuss qualitatively the effect of a single impurity.[15] A zinc impurity is a spinless ion and therefore can be described as a vacant site as depicted in Figs. 1(b) and 1(c). In other words, the bond exchange interaction $\mathbf{S}_i \cdot \mathbf{S}_j$ (in units of the exchange coupling J) acts on all bonds of the kagome lattice except on the four bonds connected to the impurity. Using Lanczos exact diagonalizations (LED) of small clusters of the kagome QHAF,[16] it has been shown that a single impurity tends to "localize" two singlet bonds next to it.[17–19] Although this local phenomenon is well captured even on very small clusters,[13] LED of the QHAF do not allow to investigate reliably the perturbation of the media at larger distances from the impurity, which can be probed, e.g., by NMR. Therefore, we shall use here an effective description based on the recently developed QDM allowing to handle larger clusters.[20,21]

B. Competing singlet phases in the pure system

Starting from a projection of the QHAF on the (nonorthogonal) nearest-neighbor (NN) singlet basis[22] (an approximate resonating VB description) followed by a transformation onto an *ad hoc* orthogonal "dimer" basis and, finally, by a series expansion (in terms of a small overlap parameter $\alpha=1/\sqrt{2}$), one gets an effective QDM of the type shown in Fig. 2. Here we use the amplitudes obtained in Ref. 21, $V_6=1/5$, $V_8=2/63$, $V_{10}=1/255$, $V_{12}=0$, $J_6=-4/5$, $J_8=16/63$, $J_{10}=-16/255$, $J_{12}=0$ (in units of J) which defines our "Heisenberg" effective QDM $H_{\rm Heis}$. For convenience, the labels γ in the amplitudes J_γ and V_γ correspond to the lengths of the associated resonance loops. An exactly solvable "Rokhsar-Kivelson" (RK) QDM $H_{\rm RK}$ defined by vanishing diagonal amplitudes $V_\gamma=0$ and equal J_γ kinetic amplitudes (set here to -1/4) has also been introduced.[23] Following Ref. 24, we shall consider a linear interpolation between the two Hamiltonians, $H_{\rm eff}(\lambda)=\lambda H_{\rm Heis}+(1-\lambda)H_{\rm RK}$. As we shall see next, it is remarkable that this "generalized" QDM can describe topological dimer liquid, VBC and the critical region on equal footing. Whether this model (for $\lambda=1$ or around this value) describes faithfully the original (unprojected) microscopic QHAF on the kagome lattice is still under debate. However, lots of insights on how impurities behave *generically* in the quantum disordered phases described by this effective model can be obtained.

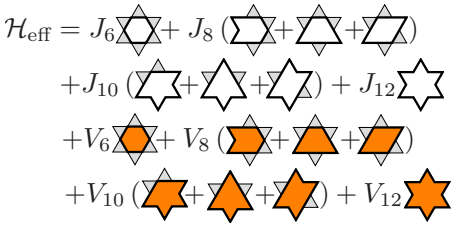

FIG. 2. (Color online) The effective QDM used here. A sum over all the hexagons of the lattice is implicit. Kinetic terms (J_γ) promote cyclic permutations of the dimers around the loops (shown as thick lines) and diagonal terms (V_γ) count the numbers of "flippable" loops.

So, prior to the introduction of impurities, let us give a brief summary of the results of the pure generalized QDM (in zero magnetic field). Generically, short- or long-range ordering of the dimers can happen yielding to dimer liquids or VBC, respectively. Numerical results[24] show that a 36-site unit cell VBC [shown schematically in Fig. 3(a)] is stabilized for $\lambda>\lambda_C\simeq 0.94$, in particular, at the Heisenberg point $\lambda=1$. A remarkable (topological) gapped $\mathbb{Z}_2$ dimer liquid which bears an exact analytical form at the RK point $\lambda=0$ is stable for $\lambda<\lambda_C$ as shown in the phase diagram of Fig. 3(b). Besides, at exactly $\lambda=1$, J_{12} vanishes so that the undetermined chiralities of the pinwheel (or star) resonances of the VBC pattern (see, e.g., Ref. 24 for details) lead to an extra (Ising-type) macroscopic degeneracy. These findings at $\lambda=1$ are in perfect agreement with recent series expansions on the QHAF.[7] Note that the proximity to a quantum critical point suggests that dimer fluctuations remain strong and that the VBC amplitude is weak at $\lambda=1$. However it should be

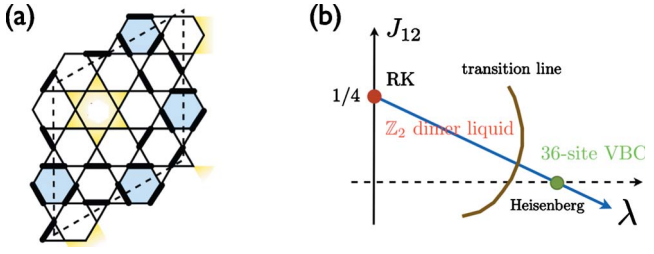

FIG. 3. (Color online) (a) Schematic representation of the 36-site VBC supercell (from Refs. 21 and 24). (b) Phase diagram of the *pure* QDM. In the present study, one moves along the (blue) λ axis.

stressed here that the derivation of the $\lambda=1$ effective QDM is only semiquantitative since it relies (i) on the projection of the Heisenberg Hamiltonian onto the singlet subspace spanned by the NN VB and (ii) it is subject to a (controlled) truncation of a series expansion. Besides, the real material might contains longer range exchange interactions. This suggests that a faithful description of the material in terms of a generalized QDM might not correspond exactly to $\lambda=1$. We can however consider λ as a "phenomenological" parameter which enables to "tune" the system in one of the two quantum disordered phases or in the critical region in between to investigate the generic role of impurities in each case.

C. Extending the QDM to finite magnetic field

Spinon hoppings. In an NMR setup a small magnetic field is applied to slightly polarize the system. The local site-dependent magnetization is then experimentally accessible via the measured Knight shift. However, ground states with finite magnetization cannot be addressed theoretically within the above QDM which only describes the singlet subspace dynamics. Nevertheless, a finite field/magnetization setup can be realized theoretically by introducing extra spin-1/2 degrees of freedom (named "spinons" hereafter) in the QDM description as first proposed in Ref. 25. Physically, such a spinon (polarized along the magnetic field) can be viewed as resulting from the breaking of a singlet bond by the introduction of a vacant site (impurity). Spinon nearest-neighbor pairs can also appear or disappear by exchanging with dimers (see below). The bond exchange interaction of the QHAF leads to the motion of the spinons followed by some dimer "backflow."[26] Since, the generalized QDM has been derived in Ref. 21 assuming a fermion representation of the (original) SU(2) dimers, consistency implies that the mutual (bare) statistics of the spinons should be fermionic.[27] Here, we extend the procedure of Ref. 21 to derive from the microscopic QHAF the simplest effective Hamiltonian (in lowest α^2 order) governing the dynamics of the (fermionic) spinons sufficient to capture the main features of spinon delocalization. The relevant processes are shown in Figs. 1(d)–1(f). The overlap matrix elements between the initial and final SU(2) configurations $|\phi\rangle$ and $|\psi\rangle$ involved in these processes are $\mathcal{O}_{\phi,\psi}=-1/2$. The corresponding Heisenberg matrix elements $\mathcal{H}_{\phi,\psi}$ equal $+1/2$ (in units of J) for the last two processes of Figs. 1(e) and 1(f) and vanishes for the first one of Fig. 1(d). Note that, for consistency with the definition of the QDM of Fig. 2, we subtract a singlet-bond energy and include a 4/3 multiplicative factor.[28] Using the expansion scheme given by (the first two terms of) Eq. (41) in Ref. 21, we deduce easily that, in the effective QDM, the first process vanishes and the two remaining kinetic processes shown in Figs. 1(e) and 1(f) involve the same "spinon hopping" amplitude $t_{\rm sp}=+1/2$. This procedure also generates (at order α^4) a potential term of amplitude $V_{\rm sp}=1/4$ which "counts" the number of possible spinon hopping of each kind. Strictly speaking, this (minimal) effective spinon Hamiltonian is most relevant to the physical case $\lambda=1$ but it is also interesting to investigate its properties in an extended range, e.g., $0.5\leq\lambda\leq 1$.

Spinon chemical potential. The density of spinons $n_{\rm sp}=N_{\rm sp}/N$ is tuned by the magnetic field H. Indeed, $N_{\rm sp}$ spinons polarized along the field gain Zeeman energy $-(h/2)N_{\rm sp}$, where $h=\frac{4}{3}g\mu_B H$, which is balanced by a creation energy term $(\Delta_{\rm B}/2)N_{\rm sp}$. Note that we rescale here the magnetic field by the same 4/3 factor as the QDM.[21,28] Physically, the parameter $\Delta_{\rm B}$ corresponds to the energy cost of breaking a singlet bond into a triplet made of two polarized *static* NN spinons.[29] Practically, $(h-\Delta_{\rm B})/2$ plays the role of a chemical potential for the spinons and the (grand canonical) GS energy becomes,

$$E_{\rm gs}(h,N_{\rm imp})=\mathrm{Min}_{/N_{\rm sp}}\left\{E_{\rm eff}[N_{\rm sp},N_{\rm imp}]-\frac{1}{2}(h-\Delta_{\rm B})N_{\rm sp}\right\}, \tag{1}$$

where $E_{\rm eff}[N_{\rm sp},N_{\rm imp}]$ is the GS energy of the QDM depicted in Fig. 2 doped with $N_{\rm sp}$ *mobile* spinons and $N_{\rm imp}$ (random) impurities and where a minimization over $N_{\rm sp}$ has been carried out. Although, strictly speaking, one expects $\Delta_B=1$ (in units of J)[28] within the procedure of Ref. 21 to derive the effective QDM, its "optimum" value for a given order of the expansion scheme is unclear. However, $\Delta_{\rm B}$ can also formally be related to the physical spin gap $\Delta_{\rm S}$ of the *pure system*, i.e., the minimal energy cost to create a triplet ($S=1$) two-spinon state in zero magnetic field (see below). Lastly, we note that two spinons can form a (triplet) bound state[30] whenever $E_{\rm eff}[2,0]+E_{\rm eff}[0,0]-2E_{\rm eff}[1,0]<0$ (in the pure system).

III. SINGLE-IMPURITY RESULTS

A. Local dimer modulation

As a preliminary study, we now start by just inserting a single spinless impurity (no spinon). As stated above, we use the modelization of the impurity in terms of a vacant site as shown in Figs. 1(b) and 1(c). In the framework of the generalized QDM, the vacancy suppresses the resonant and diagonal terms of Fig. 2 whose loop contains the vacancy site.[31]

In the very diluted impurity limit, one does not expect to fundamentally modify the *bulk* properties of the quantum magnet. However, a single impurity can, e.g., pin VBC order and, in some way, offers a very interesting probe of its existence. To test this, we have considered the $5\sqrt{3}\times 5\sqrt{3}$ periodic cluster of Fig. 4(a) with $N=75$ sites and a single impurity (to comply with the hard-core dimer constraints such a cluster has to contain an odd number of sites).[32] The full spectrum of this cluster is shown in Fig. 5(a) as a function of the parameter λ. Here we have distinguished between the four topological sectors (for such a torus topology)[33] and used the reflection symmetry with respect to one of the C_2 axis passing through the impurity site ($\sigma=\pm 1$). A quantum phase transition[34] occurs as a function of λ for $\lambda=\lambda_C\simeq 0.9373$ as evidence from the sharp peak in the GS generalized susceptibility $\chi_\lambda=\partial^2 E_{\rm GS}/\partial\lambda^2$ shown in the inset.[35] A topological $\mathbb{Z}_2$ liquid (with fourfold degeneracy on a torus) is stable for $\lambda<\lambda_C$. At $\lambda=\lambda_C$ the *single-vortex* (or "vison") gap[36] corresponding to the first odd ($\sigma=-1$) energy excitation vanishes. For $\lambda>\lambda_C$ the system spontane-

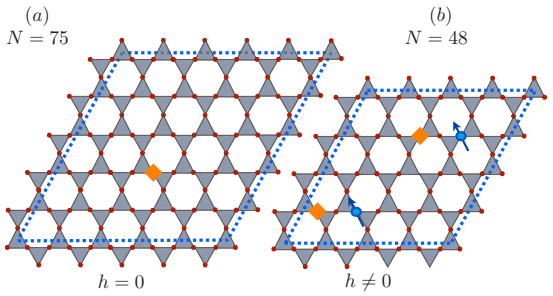

FIG. 4. (Color online) Periodic clusters used in this study; (a) the $5\sqrt{3}\times5\sqrt{3}(N=75)$ cluster with a single static impurity. (b) The $4\sqrt{3}\times4\sqrt{3}(N=48)$ cluster doped with $N_{\rm imp}=2$ static impurities and $N_{\rm sp}=2$ mobile spinons (polarized along the field).

ously breaks reflection symmetry (the GS is twofold degenerate with $\sigma=\pm1$ quantum numbers) as expected in the 36-site VBC. These results and, in particular, the estimation of the critical value $\lambda_C\simeq0.9373$ are fully consistent with the results obtained on a pure 108-site cluster.[24]

It is interesting to examine the behavior of the dimer density as a function of the Manhattan distance [see Fig. 1(c)] from the impurity, as reported in Fig. 5(b) for different values of λ between 0.5 and 1. One striking feature is the large value of the dimer density on the two bonds facing the impurity (distance $d=2$). This can be interpreted as a (singlet) *dimer crystallization* as found in prior studies of the Heisenberg quantum antiferromagnet.[17–19] Our study reveals that this phenomena is very robust and depends weakly on the supposed phase, liquid ($\lambda<\lambda_C$) or crystalline ($\lambda>\lambda_C$), of the model. Therefore this feature cannot be used practically as an experimental fingerprint. In contrast, when considering

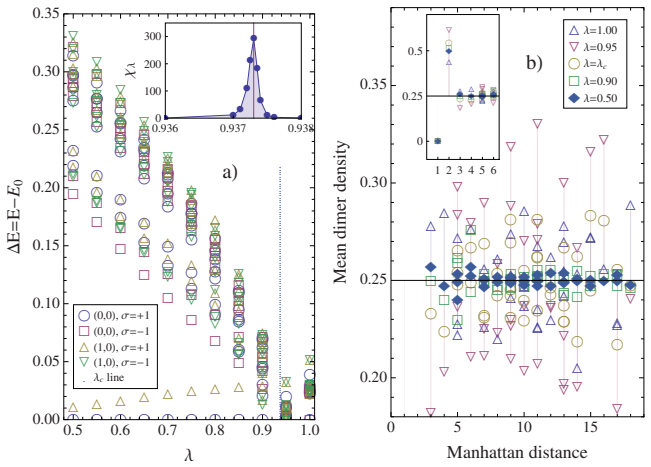

FIG. 5. (Color online) (a) Spectrum versus λ of the effective QDM on a $N=75$ site periodic cluster containing a single impurity and with zero magnetization. The eight lowest energy levels are shown in each of the four symmetry sectors. Inset: generalized susceptibility (see text) showing the location of the phase transition. For $\lambda<\lambda_c$, the large spectral gap above the quasidegenerate topological GS correspond to the single-vison gap of the $\mathbb{Z}_2$ liquid. (b) Average dimer density versus Manhattan distance from the impurity on the same $N=75$ cluster. The short-distance behavior is separated in the inset for clarity. The mean value corresponds to 1/4 dimer per bond.

longer distances, strong differences in the bond modulation occur in the supposed liquid and VBC phases. For $\lambda<\lambda_C$, in the $\mathbb{Z}_2$ dimer liquid, the dimer density becomes very uniform beyond distance 1. When increasing λ the appearance of strong modulations is exactly correlated with the crossing of the critical value and the entering in the VBC phase. For $\lambda=1$, the relative bond modulation amplitude is of order 20%.

B. Effect of a next-nearest-neighbor exchange coupling

Recent calculations using variational Gutzwiller-projected wave functions have shown that a small next-NN (NNN) ferromagnetic coupling j_2 (measured in units of the NN exchange) may favor VBC ordering.[37] A ferromagnetic coupling should then enhanced the dimer response around impurities, an effect which can be tested within the QDM framework by considering again the $N=75$ cluster doped with a single impurity (no spinon). From Ref. 21, the new QDM amplitudes J_γ and V_γ, $\gamma=6,8,10$ have simply to be multiplied by extra coefficients $(1+A_\gamma)$ which depend on j_2. A_γ is given by the ratio of the corresponding QHAF Hamiltonian matrix elements and, from Eq. (12) of Ref. 21 giving the general form of these matrix elements, one gets $A_\gamma=j_2\Sigma_{(i,j)\in\gamma,\mathrm{NNN}}\epsilon_{i,j}/(\gamma/2+\Sigma_{(i,j)\in\gamma,\mathrm{NN}}\epsilon_{i,j})$ where each loop topology has now to be distinguished and $\epsilon_{i,j}=-1(+1)$ if the sites i and j on the loop γ are separated by an odd (even) distance. Note that for $\gamma=12$ (star resonance), the NN QHAF matrix element $\gamma/2+\Sigma_{(i,j)\in\gamma,\mathrm{NN}}\epsilon_{i,j}$ vanishes so that the leading contributions to J_{12} and V_{12} are directly proportional to j_2. Using the general expansion scheme given by Eq. (41) of Ref. 21 it is straightforward to obtain the leading contribution (at order α^{10} and α^{20}, respectively), $J_{12}=-\frac{3}{8}j_2$ and $V_{12}=-\frac{3}{256}j_2$.

The excitation spectrum for $\lambda=1$ shown as a function of j_2 in Fig. 6(a) reveals two gapped phases separated by a narrow gapless region located around $j_2^c\sim0.05$ (which might become a quantum critical point in the thermodynamic limit). The $j2<j_2^c$ region (including $j_2=0$) corresponds to the above pinned VBC as confirmed by the GS quasidegeneracy and the enhanced VBC patterns shown in Fig. 6(b) for weak *ferromagnetic* j_2. In contrast, for AFM NNN exchange $j_2>j_2^c$, only a small dimerization is observed in Fig. 6(b), except at short distances from the impurity. This might be the signature of a dimer liquid or a very weakly pinned VBC and more work (on pure systems) is needed to resolve this case.

C. Does a spinon bind to an impurity?

Notoriously, spinons in dimer liquids (VBC) are known to be deconfined (confined). However, confinement/deconfinement is an asymptotic (e.g., long-distance) property of the system and unexpected behaviors can appear at shorter distance (comparable, e.g., to the typical impurity separation). Indeed, a spinon could bind to an impurity (acting here as a "static spinon") even in a dimer liquid or, reversely, a spinon could spread over a very large area (e.g., beyond the cluster sizes available numerically) even in a VBC. To investigate such issues, we now consider a $4\sqrt{3}\times4\sqrt{3}$ (48-site)

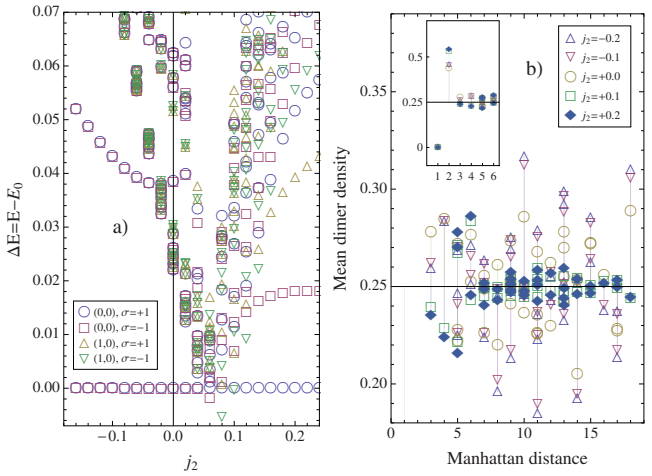

FIG. 6. (Color online) (a) Spectrum versus j_2 (NNN coupling in units of the NN coupling) of the $\lambda=1$ effective QDM on a $N=75$ site periodic cluster containing a single impurity and with zero magnetization. The lowest energy levels are shown in each of the four symmetry sectors. (b) Average dimer density versus Manhattan distance from the impurity on the same $N=75$ cluster. The short-distance behavior is separated in the inset for clarity. The mean value corresponds to 1/4 dimer per bond.

cluster[32] ($j_2=0$) doped with a static vacancy and a mobile spinon. The maps of both the (bond) dimer density and the site magnetization are shown in Fig. 7 for three distinct regimes: (i) $\lambda=0.5<\lambda_C$, deep in the dimer-liquid phase; (ii) $\lambda=0.9<\lambda_C$; and (iii) $\lambda=1>\lambda_C$, in the dimer liquid and VBC phases, respectively, in the vicinity of λ_C. The dimer density maps in this lightly polarized system closely resemble the previous zero-field data of Fig. 5(b): the dimer-liquid phase at $\lambda=0.5$ exhibits a very homogeneous dimer density apart from the two "crystallized" bonds next to the impurity while strong dimer patterns are clearly visible in the VBC phase. Note that the dimer pattern gets more pronounced in the dimer-liquid phase when approaching the dimer liquid-VBC transition, as, e.g., for $\lambda=0.9$. The local magnetization maps of Figs. 7(b) and 7(c) are entirely correlated with the dimer density maps: for $\lambda=0.9$ (liquid) the magnetization is slightly depressed on the four bonds NN to the impurity and very uniformly distributed beyond. For $\lambda=1$ (VBC) a strong modulation in the local magnetization appears. In other words, the magnitudes of the dimer and of the (magnetic field induced) spin-density modulations seem to scale with each other. The behavior in the dimer-liquid phase is fully

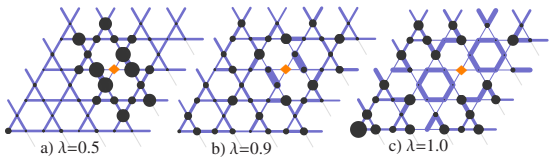

FIG. 7. (Color online) Real-space maps of the dimer density (segments) and site magnetization (circles) computed on a periodic $N=48$-site cluster doped with a single impurity and a mobile spinon, for different values of λ (as shown on the plots). The radii (width) of the circles (segments) are directly proportional to the values of the corresponding observables.

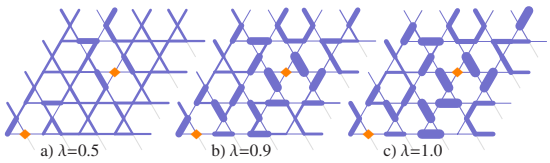

FIG. 8. (Color online) Real-space maps of the dimer density (segments) on a periodic $N=48$-site cluster doped with two impurities. Same conventions as Fig. 7.

consistent with the expected *spinon deconfinement* mechanism found by LED of small clusters of the kagome QHAF.[17,38] In contrast, the VBC sample does not seem to show *at the length scale of the cluster* the (opposite) confinement behavior found, e.g., in the VBC phase of the QHAF on the checkerboard lattice.[38]

Although probably not directly relevant to experiments, the data of Fig. 7(a), deep in the dimer-liquid phase, are of particular theoretical interest: here, although the dimer pattern is very uniform (as expected in a dimer-liquid phase) and no confining potential is expected, the spinon still forms a tight bound state with the impurity. We believe however that this behavior is not generic and depends strongly on the details of the spinon Hamiltonian: here the bound state is stabilized by an increase in spinon kinetic energy in the vicinity of the impurity. Whether such bound state can appear spontaneously without magnetic field depends on the value of the spinon chemical potential, i.e., on Δ_B. If this is the case, the impurity-doped system becomes gapless for magnetic excitations (see below).

IV. FINITE IMPURITY CONCENTRATION

We now consider the case of $N_{\rm imp}=2$ impurities doped into the same cluster of $N=48$ sites, attempting to (crudely) mimic a finite density of impurities $n_{\rm imp}=N_{\rm imp}/N$ of order 4%. For simplicity, we fix the relative position between the two impurities at a "typical" distance, as shown in Fig. 4(b). We shall also consider the same values of the parameter λ as above in the investigation of a single impurity, namely, $\lambda=0.5$, 0.9, and 1, for comparison. Hereafter, we also set $j_2=0$.

A. Enhanced dimerization

Let us first assume zero total magnetization, e.g., $N_{\rm sp}=0$. The corresponding data are shown in Figs. 8(a)–8(c). We clearly observe a sizable increase in the average dimerization compared to $N_{\rm imp}=1$. This is particularly clear for $\lambda=0.9$, a parameter corresponding, in the pure system, to the dimer-liquid phase close to the phase transition at $\lambda=\lambda_C$. In fact, with two doped impurities, the new dimerization pattern in Fig. 8(b) resemble very closely the one at $\lambda=1$ in Fig. 8(c). It is interesting to also note that the local dimerization patterns around impurities can be different. Indeed, e.g., in Figs. 8(b) and 8(c), while one impurity is surrounded by two (quasi-isolated) strong dimer bonds, the second impurity stabilizes two neighboring symmetric resonating hexagons. All these

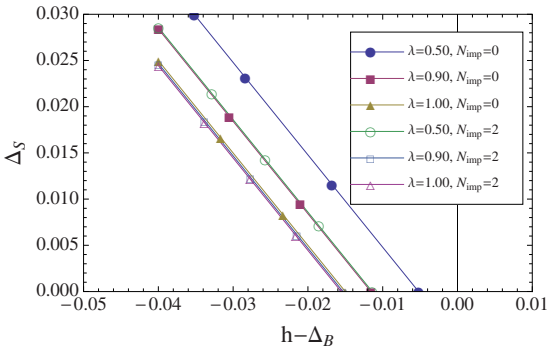

FIG. 9. (Color online) Spin gap of the pure (filled symbols) and two-impurity (empty symbols) doped 48-site cluster vs the parameter Δ_B.

findings are in fact consistent with the proposed picture of the valence-bond glass.[39]

B. Spin gap

We now consider the possibility that the ground state carries a small magnetization proportional to the (doped) spinon density $m=\frac{1}{2}n_{sp}$. If a spin gap exists at $h=0$, we expect that a large enough magnetic field will eventually suppress the gap and induce a small magnetization. In our picture, the spin gap is the minimal energy to create a pair of mobile spinons. From Eq. (1), the spin gap at low field h is therefore given by

$$\Delta_S(h,n_{imp}) = E_{eff}[2,N_{imp}] - E_{eff}[0,N_{imp}] + \Delta_B - h$$
$$= \Delta_S(0,n_{imp}) - h, \quad (2)$$

where Δ_B can be taken as a phenomenological parameter (considering the fact that our spinon hamiltonian is only a minimal model and does not include the potentially important higher-order longer-range hoppings). As in the conventional picture, the spin gap (if any) vanishes linearly at a critical field. We have numerically computed the spin gap in the same $N=48$ cluster doped with two impurities (same λ's also as above), i.e., for an impurity concentration $n_{imp}=N_{imp}/N\simeq 4\%$, and compare it to the equivalent data in the pure system ($n_{imp}=0$) in Fig. 9. Interestingly, we find that doped impurities lead to a *reduction* in the spin gap in the dimer-liquid phase, e.g., for λ=0.5. In the VBC phase the effect is much less pronounced. We believe that the existence of an impurity-spinon bound state at λ=0.5 (see above) is responsible for this trend: if spinons get bound to available impurities (see below) the energy cost to create two of them is reduced.

C. Spin-density modulations

We have also examined the spinon density map (equivalent to the local magnetization map) in the two spinon-two impurity doped $N=48$ cluster, again for the same values λ as above. The features shown in Figs. 10(a)–10(c) are consistent with our previous results for a single impurity. In the λ=0.5 dimer liquid, a spinon clearly forms a bound state around each impurity. In contrast, in Figs. 10(b) and 10(c) which we might view as some local region of a valence-bond glass,[39] spinons seem to be repelled (at short distance) from the impurities. At further distances, strong spin-density modulations are induced by a strong (average) dimerization (which reversely is weakly affected by the small magnetization of the sample).

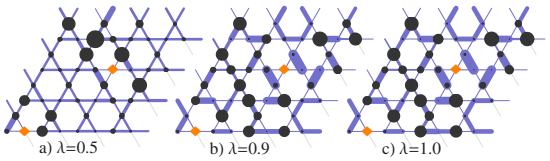

FIG. 10. (Color online) Real-space maps of the dimer density (segments) and site magnetization (circles) computed on a periodic $N=48$-site cluster doped with two impurities and two mobile spinons. Same conventions as Fig. 7.

V. APPLICATION TO NMR EXPERIMENTS

A. General considerations

The different magnetization maps in the liquid and VBC phases are expected to lead to different characteristic NMR (theoretical) spectra which can be confronted to experiments in Herbertsmithite.[12] The theoretical copper NMR spectra is defined by the histogram of the local site magnetizations. Since oxygen is located between two coppers, the effective local magnetization is obtained by summing up the contributions from both sites (named here as *bond* magnetization). Both site and bond magnetization histograms have been computed for λ=0.5, λ=0.9, and λ=1 using the spinon density maps of Figs. 7(a)–7(c) (one impurity on 48 sites) and Figs. 10(a) and 10(c) (two impurities on 48 sites) providing the theoretical copper and oxygen NMR low-temperature spectra shown in Fig. 11. Note that, for convenience, we work here at fixed magnetization[40] corresponding to one spinon per impurity, i.e., $m=\frac{1}{2}n_{imp}$. This is a natural choice at very small temperatures if spinons bind to impurities or if the spin gap is very small. In any case, this corresponds physically to a magnetic field $h>\Delta_S(h=0)$. For convenience, the copper and oxygen Knight shifts (x-axis) have been normalized with respect to the bulk values corresponding to a uniform spatial distribution of the magnetization (mimicking high temperatures). Note however that, even for such a uniform distribution of the copper spin density, the oxygen nucleus located on the bonds connected to the impurity site see only one copper atom instead of two, yielding a small satellite peak in the spectrum of Fig. 11(b) at half the bulk oxygen NMR shift.

Comparing quantitatively high- and low-temperature (in fact here $T=0$) spectra obtained at a low *fixed magnetic field* would in principle require the knowledge of the temperature-dependent magnetic susceptibility $\chi(T)$ which is beyond our numerical capability. However, a number of robust features of these theoretical NMR spectra can be linked to physical behaviors of the spinons around impurities. For example, when spinons spontaneously bind to impurities (as it is the case in the λ=0.5 dimer-liquid phase within our model), one expects low-energy magnetic excitations, possibly at arbitrary small energy scale so that the broad theoretical spectra

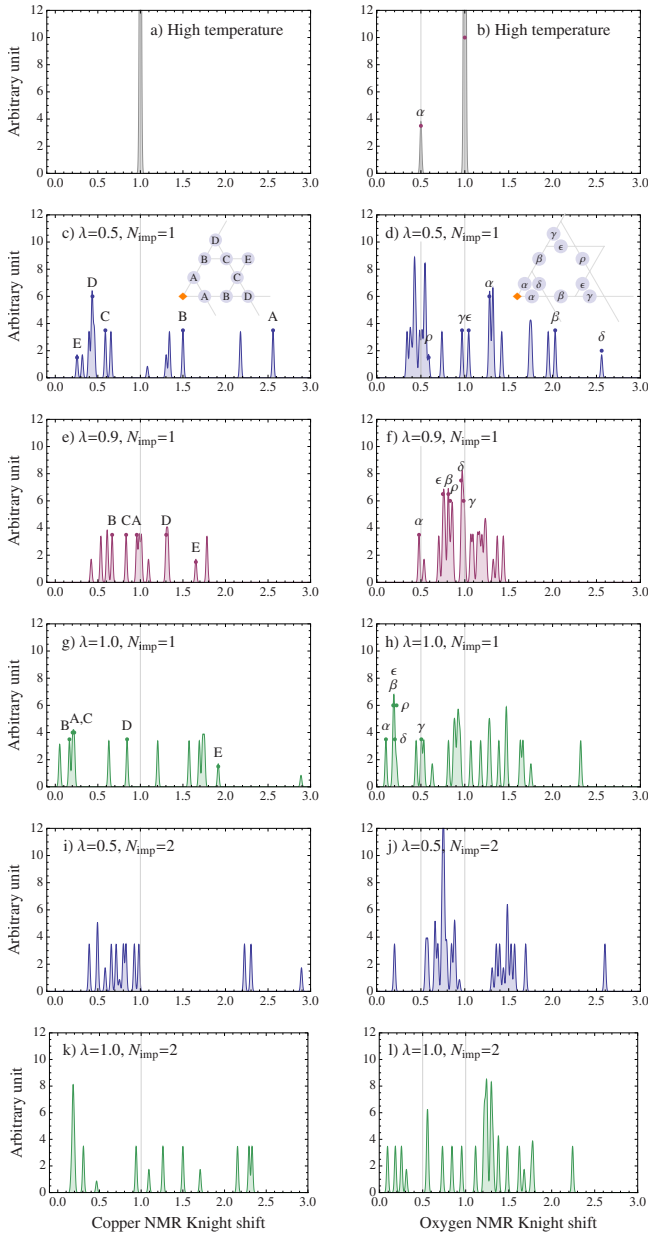

FIG. 11. (Color online) Copper (left) and oxygen (right) NMR spectra computed from the magnetization maps of Figs. 7(a)–7(c) obtained for a single impurity on 48 sites (effective concentration of ~2%) and of Figs. 10(a) and 10(c) obtained for two impurities on 48 sites (effective concentration of ~4%). The Knight shift variables are normalized with respect to the values corresponding to an ideal uniform distribution of the spin density and defining the reference NMR spectra (a) and (b) labeled as "high-temperature." Zero-temperature spectra for ~2% impurity concentration λ=0.5 (c) and (d), λ=0.9 (c) and (d) and λ=1 (g) and (h); same for ~4% impurity concentration λ=0.5 (i) and (j) and λ=1 (k) and (l). For a single impurity, the impurity peaks are labeled according to the positions of the resonating nucleus shown in the insets [see also Fig. 1(c)].

(at fixed m) of Figs. 11(c), 11(d), 11(i), and 11(j) should provide a good sketch of *low-field* NMR spectra. On the other hand, Figs. 11(e) and 11(f) correspond to the opposite case where spinons are strongly delocalized around impurities leading to narrower structures in the spectra (in the same units). However, if the system retains a finite spin gap (as expected in this type of dimer liquid), for a *small magnetic field*, the average position of the spectrum should be strongly pushed downward with respect to its high-temperature reference values.

B. Herberthsmithite described as a valence-bond glass

Let us now discuss our results in the light of the recently obtained ^{17}O NMR experimental spectra on the kagome QHAF Herberthsmithite material which contains an intrinsic small zinc substitution in the copper kagome planes.[12] Although the experimental NMR spectra are strongly broaden by quadrupolar effects typical of powders, two separate structures can clearly be followed from high to low temperatures. The average shift of the "satellite" peak is roughly half of the main one so that this peak has been interpreted as resulting from the resonance of the four oxygen nucleus (labeled as "α" in Fig. 11) next to an impurity site. Our results show that dimerization is enhanced by impurity doping so that the proposed valence-bond glass[39] should be stabilized in an enlarged interval of λ compared to the region of stability of the VBC in the pure model.

It has been recently argued that, confined spinons in the valence-bond glass can form a random-singlet phase with a wide distribution of spin gaps down to zero energy, ensuring the presence of fluctuating spins at arbitrarily low temperatures as indeed observed experimentally. The low-temperature low-field magnetic response of a valence-bond glass is therefore dominated by *isolated* impurities in rare regions of the sample, each of them carrying an almost free spinon loosely bound by a (shallow) VBC confining potential.[41] Within this scenario the $T,h\rightarrow 0$ NMR spectrum is qualitatively given by the dominant magnetic response of the above regions. If this physics is at play in Herberthsmithite, Fig. 11(h) should therefore give a crude qualitative sketch of the $T\rightarrow 0$ oxygen NMR spectrum. This spectrum vaguely shows two broad structures (as experiments) but the assignment of the small shift structure to the α oxygen is not so clear as shown in Fig. 11(h). Note that the NMR spectrum would become more complicated when raising temperature since more and more regions of the sample will contribute [as, e.g., Fig. 10(c) giving Fig. 11(l)].

VI. DISCUSSIONS AND CONCLUSIONS

Theoretically, our approach is certainly based on an approximate framework relying on (i) the truncation within the NN VB basis, (ii) an overlap expansion up to a finite order, and (iii) a "minimal" spinon effective Hamiltonian. However, we believe it still captures a number of important features and unambiguously shows that even a small (experimentally unavoidable) impurity doping should have important experimental consequences. Figure 10(c) probably gives a fairly reliable picture of what is to be expected in a small area of the experimental system at finite magnetization. Even an impurity concentration as small as 4% leads to an important increase in the average dimerization and to a fairly

inhomogeneous spin density distribution. This property should be robust in a more elaborate treatment of the NN QHAF, like, for example, when using a refined spinon Hamiltonian including longer-range hoppings.

It has been recently argued that, confined spinons in the VBC can form a random-singlet phase with a wide distribution of spin gaps,[39] ensuring the presence of fluctuating spins at arbitrarily low temperatures as indeed observed experimentally. Interestingly, our data on small clusters show that the VBC pattern is not strongly confining, probably due to the weakness of the VBC amplitude compared to the spinon kinetic energy. On the scale of the typical impurity separation, spinons tend to delocalize around impurities. However, different types of dimerization patterns get pinned around different impurities. In this sense, our findings have some similarity with the picture of the valence-bond glass.[39] Not surprisingly, we have not found any appreciable reduction in the spin gap (compared to the pure case) for the (two-) impurity configuration we have chosen (except when spinon-impurity bound states form at $\lambda=0.5$): we believe our cluster is still too small to realize (rare) configurations with isolated impurities that could exhibit (almost) free spin within some (large) confining length. This issue certainly needs further work.

On the experimental side, a more realistic description of Herbertsmithite may require to go beyond the simple NN QHAF. It is possible that longer-range exchange interactions destabilize the VBC ground state in favor of the $\mathbb{Z}_2$ dimer liquid or some other candidate GS. It might also happen that the VBC phase is only stable at temperatures lower than those experimentally reached. Finally, we note that, experimentally, a large enough DM anisotropy[11] could fill out the spin gap of the $\mathbb{Z}_2$ dimer liquid or VBC phases.

ACKNOWLEDGMENTS

We thank M. Mambrini, G. Misguich, and R. Singh for valuable discussions. We are also indebted to Fabrice Bert and Philippe Mendels for help in the understanding of their NMR data. D.P. acknowledges IDRIS (Orsay, France) for allocation of CPU time on the NEC supercomputer and A.R. acknowledges CIMENT (Grenoble, France) for access time to the local computation cluster.

[1] M. Hermele, Y. Ran, P. A. Lee, and X.-G. Wen, Phys. Rev. B **77**, 224413 (2008).
[2] P. W. Leung and Veit Elser, Phys. Rev. B **47**, 5459 (1993).
[3] H. C. Jiang, Z. Y. Weng, and D. N. Sheng, Phys. Rev. Lett. **101**, 117203 (2008).
[4] A. V. Syromyatnikov and S. V. Maleyev, Phys. Rev. B **66**, 132408 (2002).
[5] J. B. Marston and C. Zeng, J. Appl. Phys. **69**, 5962 (1991); SU(N) VBC have been introduced by N. Read and S. Sachdev, Phys. Rev. B **42**, 4568 (1990).
[6] P. Nikolic and T. Senthil, Phys. Rev. B **68**, 214415 (2003).
[7] R. R. P. Singh and D. A. Huse, Phys. Rev. B **76**, 180407 (2007).
[8] R. Budnik and A. Auerbach, Phys. Rev. Lett. **93**, 187205 (2004).
[9] M. Shores, E. Nytko, B. Bartlett, and D. Nocera, J. Am. Chem. Soc. **127**, 13462 (2005).
[10] P. Mendels, F. Bert, M. A. de Vries, A. Olariu, A. Harrison, F. Duc, J. C. Trombe, J. Lord, A. Amato, and C. Baines, Phys. Rev. Lett. **98**, 077204 (2007).
[11] A. Zorko, S. Nellutla, J. van Tol, L. C. Brunel, F. Bert, F. Duc, J.-C. Trombe, M. A. de Vries, A. Harrison, and P. Mendels, Phys. Rev. Lett. **101**, 026405 (2008).
[12] A. Olariu, P. Mendels, F. Bert, F. Duc, J. C. Trombe, M. A. de Vries, and A. Harrison, Phys. Rev. Lett. **100**, 087202 (2008).
[13] Theoretical NMR spectra have been derived on a $N=12$ sites cluster of the kagome QHAF with two impurities; see R. Chitra and M. J. Rozenberg, Phys. Rev. B **77**, 052407 (2008); M. J. Rozenberg and R. Chitra, *ibid.* **78**, 132406 (2008).
[14] K. Gregor and O. I. Motrunich, Phys. Rev. B **77**, 184423 (2008).
[15] In the very diluted limit, the magnetic response scales with the impurity concentration.
[16] For recent numerical analysis of the pure kagome QHAF, see G. Misguich and P. Sindzingre, J. Phys.: Condens. Matter **19**, 145202 (2007); P. Sindzingre and C. Lhuillier, EPL **88**, 27009 (2009).
[17] S. Dommange, M. Mambrini, B. Normand, and F. Mila, Phys. Rev. B **68**, 224416 (2003).
[18] P. Sindzingre, C. Lhuillier, and J.-B. Fouet, in *Recent Progress in Many-Body Theories*, edited by R. F. Bishop, T. Brandes, K. A. Gernoth, N. R. Walet, and Y. Xian, Advances in Quantum Many-Body Theory, Vol. 6 (World-Scientific, Singapore, 2002), p. 90; Int. J. Mod. Phys. B **17**, 5031 (2003).
[19] I. Rousochatzakis, S. R. Manmana, A. M. Läuchli, B. Normand, and F. Mila, Phys. Rev. B **79**, 214415 (2009).
[20] A. Ralko, M. Mambrini, and D. Poilblanc, Phys. Rev. B **80**, 184427 (2009).
[21] D. Schwandt, M. Mambrini, and D. Poilblanc, Phys. Rev. B **81**, 214413 (2010); note crucial differences with previous work, C. Zeng and V. Elser, *ibid.* **51**, 8318 (1995).
[22] The relevance of the NN VB basis is supported by LED of the (pure) QHAF revealing an exponential number (with N) of singlets below the spin gap, see M. Mambrini and F. Mila, Eur. Phys. J. B **17**, 651 (2000).
[23] G. Misguich, D. Serban, and V. Pasquier, Phys. Rev. Lett. **89**, 137202 (2002); see also D. S. Rokhsar and S. A. Kivelson, *ibid.* **61**, 2376 (1988).
[24] D. Poilblanc, M. Mambrini, and D. Schwandt, Phys. Rev. B **81**, 180402 (2010).
[25] A. Ralko, F. Becca, and D. Poilblanc, Phys. Rev. Lett. **101**, 117204 (2008).
[26] Z. Hao and O. Tchernyshyov, Phys. Rev. B **81**, 214445 (2010).
[27] Note the doped spinon (holon) QDM is invariant under simultaneously (i) reversing the signs of *all* kinetic amplitudes J_γ and (ii) changing the statistics of the spinons (holons) from fermionic (bosonic) to bosonic (fermionic), see D. Poilblanc, Phys. Rev. Lett. **100**, 157206 (2008) for the square lattice.
[28] We extend the rescaling of the QHAF hamiltonian of Ref. 21 to sectors with finite $S_Z=N_{\rm sp}/2$ as $\hat{\mathcal{H}}_H \rightarrow (4/3)\hat{\mathcal{H}}_H + J(N-N_{\rm sp})/2$.

[29] B. Normand, Contemp. Phys. **50**, 533 (2009).
[30] A priori binding of two spinons does not necessarily require asymptotic confinement and can take place in a deconfined spin-liquid phase.
[31] Other local resonances induced by the impurity itself exist but have negligible effects.
[32] The 48-site and 75-site clusters used here possess all the point group symmetries of the (infinite) kagome lattice. Although they do not accommodate the VBC 36-site cell, they still capture correctly the local physics around impurities. The largest Hilbert spaces are obtained for a single impurity in 75 sites (4 194 304 symmetrized states) and for two spinons and two impurities in 48 sites (8 511 488 states).
[33] The (0,1), (1,0), and (1,1) sectors are degenerate. See Ref. 24.
[34] This class of dimer liquid-VBC quantum phase transition can be described by a specific field theory, see C. Xu and S. Sachdev, Phys. Rev. B **79**, 064405 (2009).
[35] S. Chen, L. Wang, Y. Hao, and Y. Wang, Phys. Rev. A **77**, 032111 (2008).
[36] This contrasts with the case of the pure system where the spectral gap corresponds to a *double-vison* excitation. See Ref. 24.
[37] O. Ma and J. B. Marston, Phys. Rev. Lett. **101**, 027204 (2008).
[38] D. Poilblanc, A. Läuchli, M. Mambrini, and F. Mila, Phys. Rev. B **73**, 100403(R) (2006); see Fig. 4(b) of this reference.
[39] R. R. P. Singh, Phys. Rev. Lett. **104**, 177203 (2010).
[40] Instead, imposing the magnetic field would require the knowledge of the field (and temperature) dependence of the macroscopic magnetization.
[41] In that case, the bound state size is relatively large so that the 48-site cluster with a single impurity is still too small to observe real confinement.